BRL R 1580

BRL

AD

REPORT NO. 1580

NUMERICAL EXPERIMENTS TO INTEGRATE THE NAVIER-STOKES EQUATIONS

by

Clarence W. Kitchens, Jr.

April 1972

U.S. ARMY ABERDEEN RESEARCH AND DEVELOPMENT CENTER
BALLISTIC RESEARCH LABORATORIES
ABERDEEN PROVING GROUND, MARYLAND

45

Destroy this report when it is no longer needed.
Do not return it to the originator.

Secondary distribution of this report by originating or sponsoring activity is prohibited.

Additional copies of this report may be purchased from the U.S. Department of Commerce, National Technical Information Service, Springfield, Virginia 22151

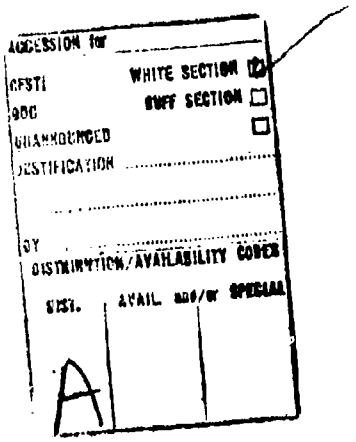

The findings in this report are not to be construed as an official Department of the Army position, unless so designated by other authorized documents.

Unclassified
Security Classification

DOCUMENT CONTROL DATA - R & D

(Security classification of title, body of abstract and indexing annotation must be entered when the overall report is classified)

1. ORIGINATING ACTIVITY (Corporate author) US Army Aberdeen Research & Development Center Ballistic Research Laboratory Aberdeen Proving Ground, Maryland 21005	2a. REPORT SECURITY CLASSIFICATION Unclassified 2b. GROUP NA

3. REPORT TITLE

Numerical Experiments to Integrate the Navier-Stokes Equations

4. DESCRIPTIVE NOTES (Type of report and inclusive dates)

NA

5. AUTHOR(S) (First name, middle initial, last name)

Clarence W. Kitchens, Jr.
Captain, Army

6. REPORT DATE	7a. TOTAL NO. OF PAGES	7b. NO. OF REFS
April 1972	55	14

8a. CONTRACT OR GRANT NO.	9a. ORIGINATOR'S REPORT NUMBER(S)
b. PROJECT NO. RDT&E 1T061102B11A	BRL Report No. 1580
c.	9b. OTHER REPORT NO(S) (Any other numbers that may be assigned this report) NA
d.	

10. DISTRIBUTION STATEMENT

Approved for public release; distribution unlimited.

11. SUPPLEMENTARY NOTES	12. SPONSORING MILITARY ACTIVITY
NA	U.S. Army Materiel Command Washington, DC

13. ABSTRACT

A series of numerical experiments are described which solve for the time dependent flow field around a circular cylinder accelerated to supersonic speeds. This study is performed using a computer program developed by Scala and Gordon which models the full time-dependent Navier-Stokes equations. Results are presented for Mach two flow past a cylinder at freestream Reynolds numbers of 15.0, 46.8, 157.2, and 704.6, based on cylinder diameter.

The numerical results are compared with analytical solutions and experimental measurements and the accuracy of the numerical results is discussed. These comparisons show where our numerical solutions of the Navier-Stokes equations fail to give accurate results.

DD FORM 1 NOV 68 1473 REPLACES DD FORM 1473, 1 JAN 64, WHICH IS OBSOLETE FOR ARMY USE.

Unclassified
Security Classification

Unclassified

Security Classification

14. KEY WORDS	LINK A		LINK B		LINK C	
	ROLE	WT	ROLE	WT	ROLE	WT
Aerodynamics						
Fluid Mechanics						
Numerical methods						
Finite-difference techniques						
wake						
Separated flow						
Shock wave						
Boundary layer						
Navier-Stokes equations						
Compressible flow						

Security Classification

B A L L I S T I C R E S E A R C H L A B O R A T O R I E S

BRL REPORT NO. 1580

APRIL 1972

NUMERICAL EXPERIMENTS TO INTEGRATE THE NAVIER-STOKES EQUATIONS

Clarence W. Kitchens, Jr.

Applied Mathematics Division

RDT&E Project No. 1T061102B11A-05

A B E R D E E N P R O V I N G G R O U N D, M A R Y L A N D

BALLISTIC RESEARCH LABORATORIES

BRL REPORT NO. 1580

CWKitchens/ngh
Aberdeen Proving Ground, Md.
April 1972

NUMERICAL EXPERIMENTS TO INTEGRATE THE NAVIER-STOKES EQUATIONS

ABSTRACT

A series of numerical experiments are described which solve for the time-dependent flow field around a circular cylinder accelerated to supersonic speeds. This study is performed using a computer program developed by Scala and Gordon which models the full time-dependent Navier-Stokes equations. Results are presented for Mach two flow past a cylinder at freestream Reynolds numbers of 15.0, 46.8, 157.2, and 704.6, based on cylinder diameter.

The numerical results are compared with analytical solutions and experimental measurements and the accuracy of the numerical results is discussed. These comparisons show where our numerical solutions of the Navier-Stokes equations fail to give accurate results.

TABLE OF CONTENTS

LIST OF ILLUSTRATIONS

LIST OF SYMBOLS

c_v	Specific heat at constant volume [Ft-lb_f/lb_m - ^oR]
g	Gravitational constant [lb_m - ft/lb_f - sec^2]
k	Thermal conductivity [lb_f / ^oR - sec]
m	Stretching factor for difference mesh [nondimensional]
n	Number of time steps [nondimensional]
p	Thermodynamic pressure [lb_f/ft^2]
s_1	Outer boundary defined by equation (11) [ft]
t	Time [sec]
u_i	Cartesian velocity components [ft/sec]
x	Angular coordinate defined by equation (12) [nondimensional]
x_i	Cartesian coordinates [ft]
D	Comoving derivative
M	Mach number [nondimensional]
R	Radial coordinate [ft]
$\bar{R}$	Gas constant [ft-lb_f/lb_m-^oR]
R_o	Cylinder radius [ft]
R_2	Distance along $\theta = 0^o$ from center of cylinder to outer boundary [ft]
Re_d	Freestream Reynolds number based on cylinder diameter [nondimensional]
T	Temperature [^oR]
U	Radial velocity component [ft/sec]
V	Tangential velocity component [ft/sec]
X	Distance downstream from center of cylinder [ft]
Y	Distance above center of wake [ft]
α	Mesh spacing constant in coordinate transformation (13) [nondimensional]
γ	Ratio of specific heats [nondimensional]
δ_{ij}	Kronecker delta [nondimensional]
η	Transformed coordinate (14) [nondimensional]
θ	Angular coordinate [radians]
λ	Second coefficient of viscosity [lb_f-sec/ft^2]
λ_o	Mean free path at freestream conditions [ft]

μ First coefficient of viscosity [lb_f - sec/ft^2]

ξ Transformed coordinate (13) [nondimensional]

π Constant (3.1415926536) [nondimensional]

ρ Density [lb_m/ft^3]

ρ_2 Density behind the bow shock [lb_m/ft^3]

τ Time constant ($\tau = t\, U_\infty / 2\, R_o$) [nondimensional]

τ_{ij} Stress tensor [lb_f/ft^2]

Subscript

∞ Freestream conditions

I. INTRODUCTION

This report describes a series of numerical experiments based on a computer program developed at the General Electric Company by Scala and Gordon[1*]. This program which is based on the full time-dependent Navier-Stokes equations is used to calculate the flow field around a circular cylinder accelerated to a supersonic velocity. The validity of our numerical results is determined by comparison with analytical solutions and experimental wake measurements.

Accurate numerical solutions of the full Navier-Stokes equations are desirable for many problems in weapons technology. For problems like the internal flow in fluidic devices or the wake flow behind a ballistic missile the simplifying assumptions of inviscid flow or high Reynolds number boundary-layer flow are not applicable. To describe the flow field in such problems it is possible to resort to numerical solution of the full Navier-Stokes equations.

Several numerical solutions of the Navier-Stokes equations have been published for compressible viscous flows, such as those of Crocco[2], Thommen[3], Scala and Gordon[4], Allen and Cheng[5], and Trulio and Walitt[6,7]. The flow detail exhibited in these solutions is quite remarkable, but in certain regions of the flow field the numerical solutions may not be very accurate. At the present time we should accept the results of any such numerical computation with great caution since the mathematical theory on which the numerical solution is based is inadequate. There are no rigorous proofs of stability or convergence of the numerical methods employed for these solutions, nor are there any proofs of uniqueness. It is necessary to assess the validity of any such numerical computation by comparing it against known analytical solutions and experimental measurements.

Results are presented for Mach two flow past circular cylinders at Reynolds numbers 15.0, 46.8, 157.2, and 704.6. The numerical solutions are compared with analytical solutions for the density ratio

---

* References are listed on page 48

across the bow shock, shock structure, and shock standoff distance. The validity of the cylinder wake-region calculations is determined by comparison with experimental hot-wire wake measurements[8].

II. FORMULATION OF THE PROBLEM

The governing equations on which our numerical solutions are based are formulated within the framework of classical continuum mechanics. The Navier-Stokes equations are formed from Cauchy's First Law of Continuum Mechanics

$$\rho \frac{Du_i}{Dt} = g \frac{\partial \tau_{ji}}{\partial x_j} \quad , \tag{1}$$

when the stress tensor τ_{ij} is expressed as a linear function of the deformation gradient. We thus assume

$$\tau_{ij} = \left(- p + \lambda \frac{\partial u_m}{\partial x_m} \right) \delta_{ij} + \mu \left(\frac{\partial u_i}{\partial x_j} + \frac{\partial u_j}{\partial x_i} \right) . \tag{2}$$

The basic equations have been written here in Cartesian tensor notation for simplicity. The viscosity coefficients appearing in equation (2) are further assumed to be related by Stokes postulate

$$3\lambda + 2\mu = 0 . \tag{3}$$

Equation (3) can be shown to be valid for monotomic ideal gases. The Navier-Stokes equations give us three equations to relate the six field functions. We also use the continuity equation

$$\frac{D\rho}{Dt} + \rho \frac{\partial u_i}{\partial x_i} = 0 , \tag{4}$$

the energy equation

$$\rho c_v \frac{DT}{Dt} + p \frac{\partial u_i}{\partial x_i} = \frac{\partial}{\partial x_i} \left(k \frac{\partial T}{\partial x_i} \right) + \lambda \left(\frac{\partial u_i}{\partial x_i} \right)^2 + \mu \frac{\partial u_i}{\partial x_m} \left(\frac{\partial u_i}{\partial x_m} + \frac{\partial u_m}{\partial x_i} \right) , \tag{5}$$

and the equation of state for a perfect gas

$$p = \rho RT \ . \tag{6}$$

In this study the time-dependence in equations (1), (4), and (5) is retained and we seek steady-state solutions of the governing equations by time-wise integration from a prescribed initial state. The steady state is thus approached asymptotically with time.

The partial derivatives in the governing equations (1) thru (6) are replaced by differences in both space and time. This approximation reduces the system of nonlinear partial differential equations to a system of nonlinear algebraic equations which can be solved by numerical iteration. The set of difference equations used in this procedure was developed by Scala and Gordon[1].

The complete system of equations is formulated in general two-dimensional orthogonal coordinates. This system of equations together with their difference approximations are listed by Scala and Gordon[1]. In the present study we consider time-dependent flow past a cylinder using cylindrical coordinates (R,θ) with θ measured from the forward stagnation point.

III. DIFFERENCE EQUATIONS

The complete set of difference equations used in the computer program to approximate the governing equations are discussed in detail by Scala and Gordon[1]. The procedure followed is to split the full system of governing equations into "hyperbolic" subsystems and parabolic terms which are differenced separately and then combined into a final set of difference equations.

The second-order viscous terms, the parabolic terms, are differenced using an alternating explicit-implicit scheme[9]. At every time step the calculation at each interior point is alternated between an implicit formula and an explicit formula. According to this procedure implicit equations are used for the calculations at every alternate interior mesh point (with respect to both R and θ) at

time $t = (n)\,\Delta t$. At the remaining interior mesh points explicit equations are used for time $t = (n)\,\Delta t$. A time $t = (n+1)\,\Delta t$ the explicit points of the previous time step become implicit and vice versa. This procedure then repeats for subsequent time steps.

The "hyperbolic" subsystems are made up of both the inviscid terms and the lower order viscous terms. These "hyperbolic" terms are differenced by transforming them to diagonal form and then differencing them according to the sign of the characteristics. The calculations for these terms are then alternated between explicit and implicit equations in the same manner as described for the second-order terms.

The set of difference equations used in these calculations and the manner in which they are numerically integrated introduced several uncertainties into the accuracy of the numerical solutions. In the present difference formulation the first-order nonlinear terms involving spatial derivatives of $\mu(T)$ and $k(T)$ in the momentum equations are treated like hyperbolic terms. These terms do not necessarily remain hyperbolic throughout the flow field. The amount of error introduced into the steady-state solutions by this approximation cannot be evaluated.

The second uncertainty arises from the implicit evaluation of the second-order cross-product derivatives ($\partial^2 U/\partial R \partial\theta$, etc.). These derivatives are approximated at alternate time steps by assuming that implicit quantities are known from the previous time step. This simplification eliminates the iterations needed if the true implicit equations were used at each alternate time step. This procedure introduces some uncertainty into the time-dependence exhibited by the numerical solution. It is not known what effect, if any, this procedure has on the final steady-state numerical solution which is obtained asymptotically with time.

IV. INITIAL CONDITIONS AND BOUNDARY CONDITIONS

The treatment of the time-dependent Navier-Stokes equations requires the specification of both initial conditions (t=0) throughout the flow field and boundary conditions (t > 0) on all boundaries. Figure 1 gives a schematic representation of the flow field surrounding a cylinder traveling at supersonic speed. The flow field is characterized by a region far upstream of the body in which viscous effects are negligible. There are two shock regions in the flow field; the bow shock and the wake shock regions. Near the surface of the cylinder viscous effects become predominate and this region is characterized by a viscous layer which merges into a wake region downstream. In the wake region neither inviscid nor boundary-layer considerations are valid.

For times ≤ 0 in our numerical computations we assumed a uniform flow having freestream conditions throughout the flow field. For times t > 0 the velocity components on the surface of the cylinder were brought linearly to zero and held at this value. The following velocity boundary conditions were specified on the cylinder's surface

$$U(\theta_i) = \beta U_\infty(\theta_i) \ , \qquad V(\theta_i) = \beta V_\infty(\theta_i) \ ; \tag{7}$$

where

$$\beta = \begin{cases} (t_1 - t)/t_1 & \text{for } 0 \le t \le t_1 \ , \\ 0 & \text{for } t > t_1 \ . \end{cases} \tag{8}$$

For times $t \ge t_1$ we thus specify the no-slip condition on the surface of the cylinder.

Physically, the process of initialization described by (7) and (8) treats two different types of initial conditions. If t_1 is less than the time step Δt used in the numerical integration, then we model a cylinder impulsively accelerated from rest. If $t_1 > \Delta t$ we treat flow past a porous cylinder with the amount of mass flux through the surface decreasing to zero between times t=0 and $t=t_1$.

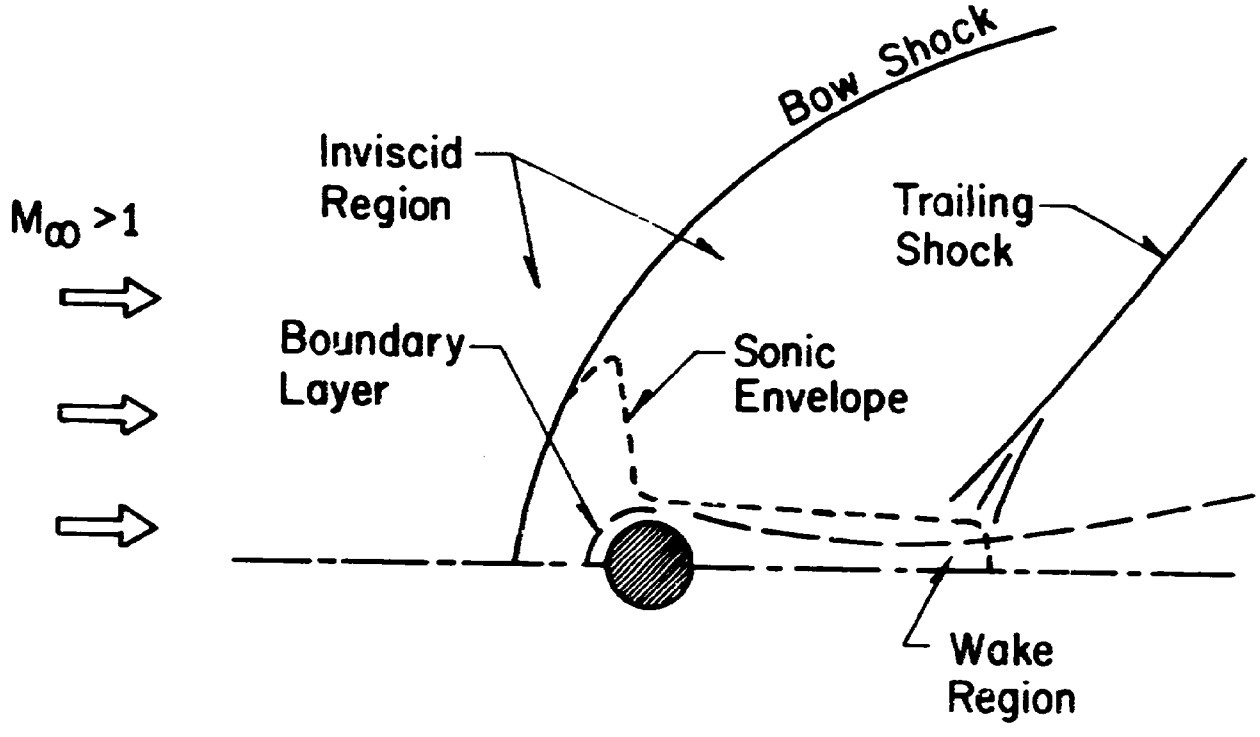

Figure 1. Schematic Representation of Flow Field Surrounding Circular Cylinder

In the latter case, for times $t < t_1$, mass exits the downstream surface of the cylinder into the flow field. We specify the density of this mass to be

$$\rho = \frac{\rho_\infty}{4} (3 + \beta) \tag{9}$$

for times $0 \leq t < t_1$. The procedure followed by Scala and Gordon[1] for specifying density boundary conditions is that whenever the flow enters the computation region through a boundary the density must be specified as a boundary condition, otherwise it is calculated at that boundary. The results of our calculations show that this boundary condition may be incorrect but it is not known whether the problem is properly posed as stated.

The boundary condition for the temperature on the cylinder's surface is specified by the assumption of an adiabatic wall

$$\left(\frac{\partial T}{\partial R}\right)_{R = R_o} = 0 \ . \tag{10}$$

It is hoped that the time-dependent history of the solution resulting from these initialization procedures will have a physical counterpart. It is assumed, however, that the resulting steady-state solution will be unique, independent of the initialization process prescribed. This assumption, unfortunately, cannot be verified analytically.

In our computations we choose the steady state from observations of the time-dependent flow in the bow shock and wake regions. At time zero the bow shock forms adjacent to the cylinder and then propagates upstream, gradually reaching a standoff distance which does not change appreciably with time. The wake flow then establishes itself after the bow shock has reached its steady-state position. After the bow shock is stationary we monitor the wake flow until this flow is invariant, or almost so, after several hundred time steps. The flow field at this stage is then said to represent the steady-state

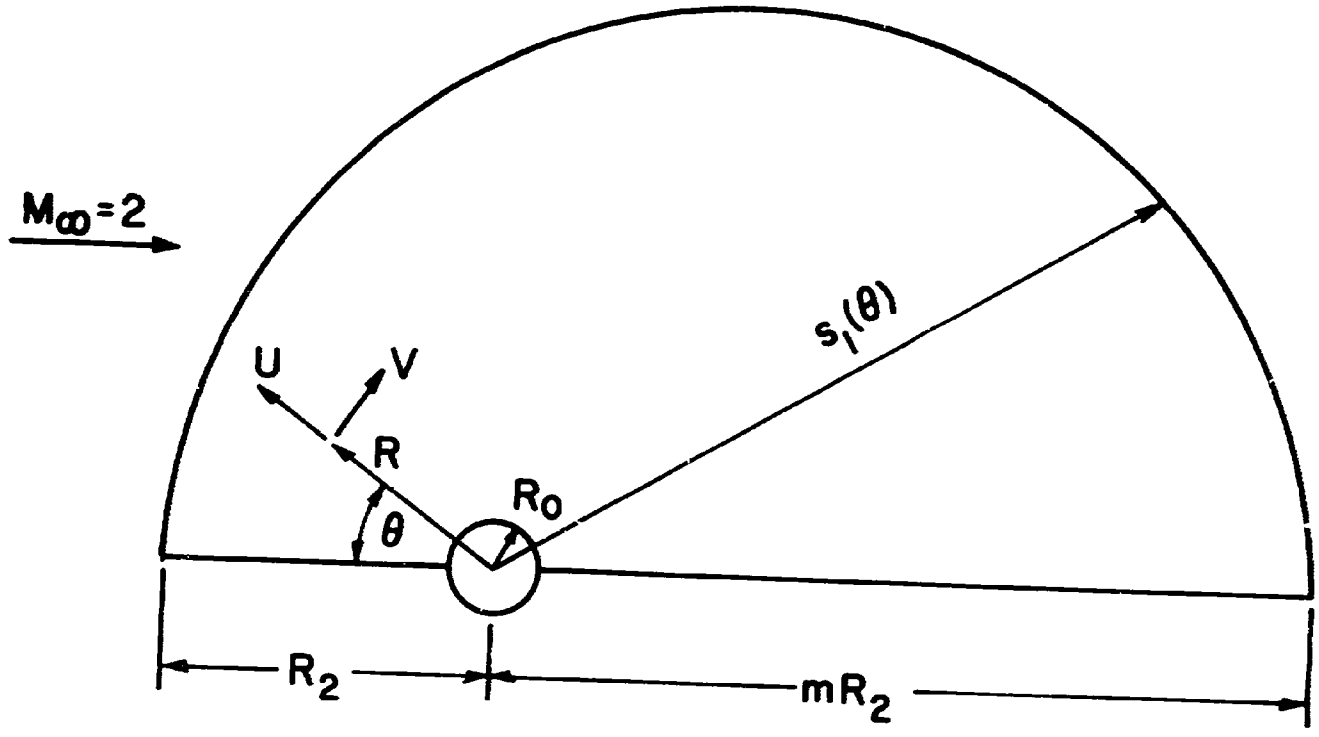

Figure 2. Region of Computation With m = 2.5

solution.

The specification of boundary conditions far from the cylinder poses a difficult numerical problem. We have used two different techniques in this study in an attempt to determine the influence of these boundary conditions on the accuracy of the numerical solution. The first method follows that used by Scala and Gordon[1]. We specify "artificial" boundary conditions along an outer boundary located at a finite distance from the cylinder's surface. The second technique has been used by Sills[10]. In this method a coordinate transformation is used to map the interval $[0,\infty]$ of R onto a finite interval [0 1]. The proper boundary conditions at infinity can then be specified at the boundary of the transformed region. Table AI shows which method was used for each calculation.

In the former case, with the outer boundary located at a finite distance from the cylinder, we prescribe the outer boundary to be

$$s_1 = R_2 \left[1 + 4\,(m-1)\,x^3 - 3\,(m-1)\,x^4\right]; \tag{11}$$

where

$$x = \frac{\theta}{\pi} \,. \tag{12}$$

The value m determines the degree of difference mesh stretching downstream of the cylinder. Our calculations were carried out for m = 2.5. With this value of m the outer boundary downstream of the cylinder ($\theta = 180^\circ$) is two and one-half times farther from the cylinder than at $\theta = 0^\circ$. Figure 2 shows a schematic of the region of computation with m = 2.5. Transformation (11) facilitates the use of a fine difference mesh upstream in the bow shock region and a coarse mesh downstream in the wake region.

For those calculations in which the mapping was employed, the radial coordinate was transformed by

$$\xi = 1 - e^{-\alpha(R-R_o)} \,. \tag{13}$$

The arbitrary constant α is a stretching factor which determines the location of the image points. This transformation permits the

specification of boundary conditions at infinity while allowing the interior grid points to be concentrated near the cylinder. It should be noted that the use of this transformation results in a solution which is inherently asymptotic at the outer boundary. As long as the derivative $\partial/\partial\xi$ remains bounded as $\xi \to 1$ in the computational plane, then $\partial/\partial R \to 0$ as $R \to \infty$. This inherent asymptotic behavior may unnecessarily result in an overspecification of boundary conditions in the numerical computation.

In our numerical solution we have made a symmetry assumption about the flow field in order to reduce the computer storage requirements and computation time. We assume a plane of reflective symmetry bisecting the cylinder's cross section and numerically treat flow in the upper half plane $0 \leq \theta \leq \pi$ . . We thus specify symmetry boundary conditions along boundaries at $\theta = 0$ and $\theta = 180^{\circ}$. The symmetry conditions prescribed on these boundaries are

$$\frac{\partial U}{\partial \theta} = 0, \quad \frac{\partial T}{\partial \theta} = 0 \text{ and } V = 0 \ . \tag{14}$$

No boundary condition was prescribed for the density on these boundaries for the calculations with a finite outer boundary (11). This follows the procedure used by Scala and Gordon[1]. For the calculations using the mapping (13) we additionally specified

$$\frac{\partial \rho}{\partial \theta} = 0 \tag{15}$$

along the boundaries at $\theta = 0^{\circ}$ and $\theta = 180^{\circ}$.

In all calculations we prescribed freestream velocity components and freestream temperature along the outer boundary, whether using (11) or (13). Freestream values were specified for density at the outer boundary whenever the flow at a boundary point was directed into the computation region when using (11). For the calculation using the mapping (13) freestream values for density were always specified at infinity.

Figure 3 shows the domain of computation and boundary conditions for two of the cases calculated using the finite outer boundary (11). The boundary conditions specified on each boundary are shown in this figure. The two outer boundaries shown in this figure correspond to their locations for the calculations performed for $Re_d = 46.8$.

V. DESCRIPTION OF COMPUTATIONS

Numerical computations were performed for Mach two flow past circular cylinders at freestream Reynolds numbers of 15.0, 46.8, 157.2 and 704.6, based on cylinder diameter. Appendix A contains the dimensional values assigned to the flow field variables for each case. Each case will be referenced by its approximate freestream Reynolds number. The four cases for a Reynolds number of 46.8 are differentiated by a suffix (i.e. 47-1, 47-2, 47-3 and 47-4).

The largest cylinder considered had a diameter of approximately one-half inch ($Re_d = 704.6$). The calculations for this case represent an upper limit of the type of calculation that can be performed in a reasonable amount of computer time using this computer program. All calculations were performed on the BRLESC II computer at the Ballistic Research Laboratories.

The difference mesh was constructed so that the angular spacing remained constant at

$$\Delta\theta = (\pi/30) = 6^\circ \tag{16}$$

for all computations. The length of a mesh element in the radial direction varied with the different computations. The smallest mesh was employed in case 47-1 for flow past a 3.056×10^{-3} ft diameter cylinder with $\Delta R = 1.030 \times 10^{-4}$ ft along the forward stagnation streamline. The largest mesh occurred in calculations such as case 47-3 which used transformation (13). In such cases the mesh elements farthest from the cylinder stretched from some finite radial coordinate to infinity. The radial mesh variation was chosen by specifying α in transformation (13) so that there would be several mesh points per

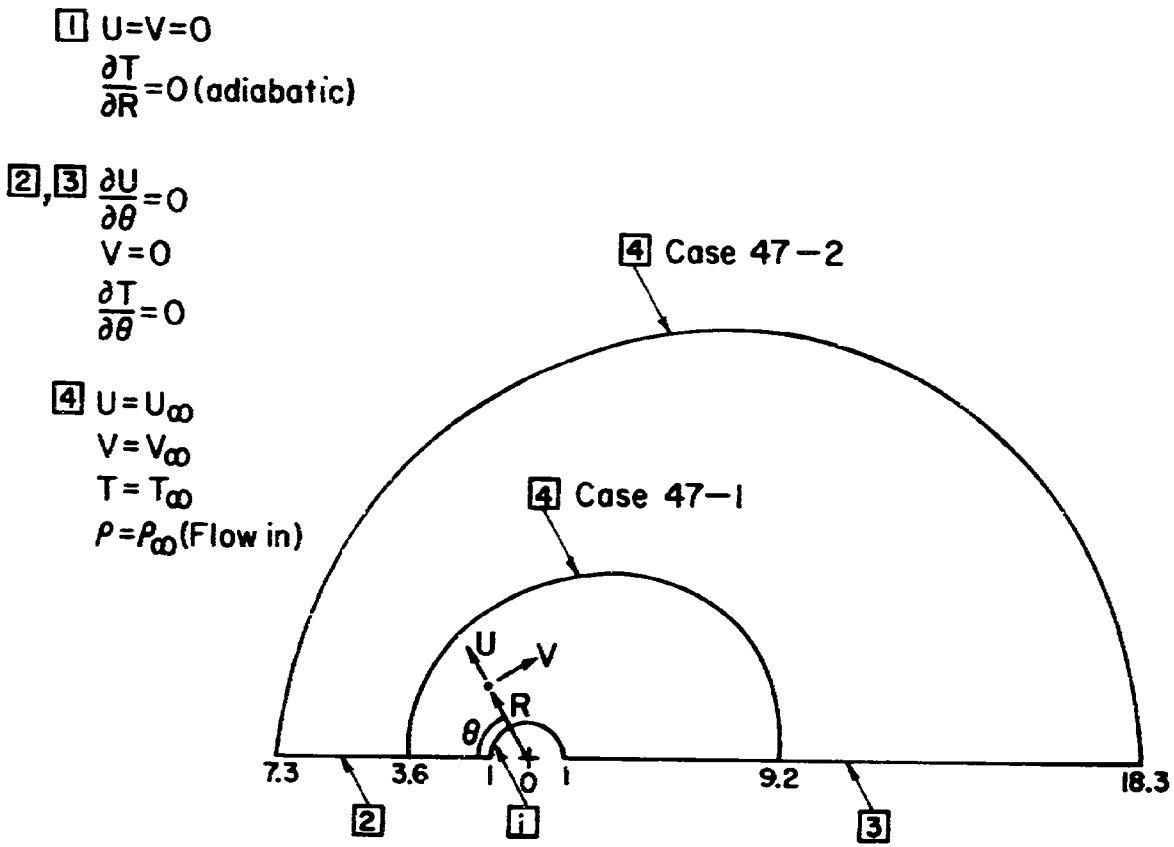

Figure 3. Domain of Computation and Boundary Conditions

freestream mean free path across the bow shock at all times.

A. $Re_d = 704.6$

The calculations for $Re_d = 704.6$* were initialized from time zero. The velocity components on the surface of the cylinder were brought linearly from their freestream value to zero in a period of 6 μsec ($t_1 = 6 \times 10^{-6}$ sec). The boundary conditions prescribed for this case are those used with the finite outer boundary.

This case was run from time zero to a non-dimensional time of $\tau = 4.80$ at which time the flow field was still unsteady. These calculations required approximately 40 hours of computer time on BRLESC II. On the basis of the shock speed and standoff distance at $\tau = 4.80$ was estimated that an additional 30 to 40 hours of computer time would be required before the flow field would reach steady-state conditions. The calculations for this case were not carried beyond this point.

A particular difficulty arose with the density calculations at the forward stagnation point on the cylinder. The density at the forward stagnation point increased rapidly with time from its freestream value at time zero, reaching a peak value approximately 12 times the freestream density at t = 6 μsec. Figure 4 shows the density variation in the vicinity of the forward stagnation point for the first 12 μsec. For times after t = 6 μsec the density at the forward stagnation point decreased monotonically with time. At t = 12 μsec the stagnation point density had decreased to approximately seven times the freestream value.

A second calculation was run for this case with $t_1 = 3$ μsec, one-half the value used previously. The peak stagnation point density

* *The calculations for this case were performed by Dr. Paul Gordon while a summer employee at the BRL. He adapted his original computer program[1] to BRLESC II and checked it for compatibility with our computer by running a previously computed case.*

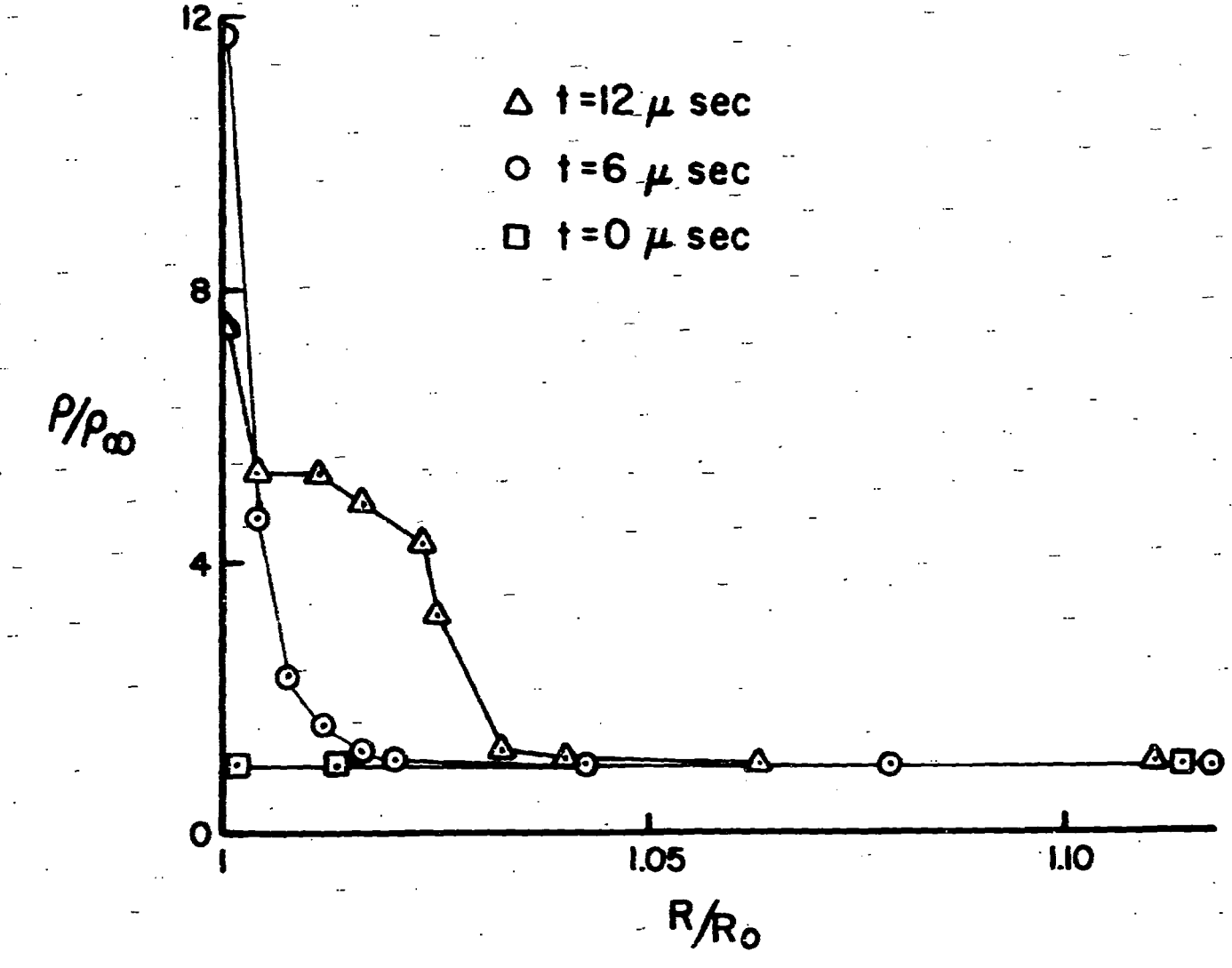

Figure 4. Density Along Stagnation Streamline ($\theta = 0^{c}$) for $Re_d = 704.6$

was lowered by approximately two percent, but now occurred at t = 3 μsec instead of t = 6 μsec. These two calculations show that the time history of the stagnation point density is quite dependent on the initialization process prescribed.

The peak values of the density predicted at the foward stagnation point are incorrect. Figure 4 shows that there is a density discontinuity for t = 12 μsec at the forward stagnation point. This discontinuity results because the numerical computations do not satisfy the symmetry condition

$$\frac{\partial \rho}{\partial \theta} = 0 \tag{17}$$

along $\theta = 0^{\circ}$. By additionally specifying (17) this discontinuity is eliminated.

B. $Re_d = 46.8$

Three sets of steady-state numerical solutions were obtained for $Re_d = 46.8$. These calculations were for a cylinder of approximately 1/32 inch diameter. The first case (47-1) was started at time zero and run until the steady-state solution was reached at $\tau = 26.2$ after approximately 3100 time steps. This case required 13 hours of computer time on BRLESC II. Figure 3 shows the placement of the outer boundary used for case 47-1.

A second calculation (47-2) was run to evaluate the effect of specifying freestream conditions at the outer boundary. For this second case the outer boundary was placed farther from the cylinder than in the first case as is shown in Figure 3. This case was initialized at $\tau = 26.2$ by interpolating from the steady-state flow field of case 47-1. The governing equations were then integrated in time until a new steady-state solution was reached for this boundary location. This required approximately 2200 additional time steps. The numerical solution achieved a new steady state at $\tau = 42.1$ after 18 additional hours of computer time.

The first two cases (47-1 and 47-2) used the boundary conditions described previously for use with a finite outer boundary. No additional density boundary conditions were specified. The calculations for case 47-1 were initialized with $t_1 = 2$ μsec. A value of t_1 was not necessary for case 47-2 since it was started by interpolation at $\tau = 26.2$.

The third case (47-3) employed the coordinate mapping (13) with the outer boundary at infinity. In this case we additionally specified a symmetry condition for the density.

$$\frac{\partial \rho}{\partial \theta} = 0 \tag{18}$$

along the boundaries at $\theta = 0^\circ$ and $\theta = 180^\circ$. This case was started at time zero with $t_1 < \Delta t$ and thus treated a cylinder impulsively accelerated from rest. The steady-state solution was reached at $\tau = 39.08$ after 12 hours of computer time and approximately 2900 time steps.

None of the steady-state solutions for $Re_d = 46.8$ predicted separation. The effect of the downstream symmetry conditions on the numerical solutions could not be determined from these calculations. In order to determine if the symmetry boundary conditions were restricting "numerical separation" a fourth case 47-4 was run.

Case 47-4 was set-up with a difference mesh surrounding the cylinder ($0 \leq \theta \leq 360^\circ$). The number of mesh elements used was twice that of case 47-3. The mesh size was identical to that used in case 47-3. This 360° placement of nodes eliminated the necessity for the specification of downstream symmetry conditions. This case was started at time zero in the same manner as case 47-3 and run to a non-dimensional time $\tau = 7.90$. A comparison of cases 47-3 and 47-4 showed them to be almost identical at each time step and it was concluded that their steady-state solutions would be the same. The calculations for case 47-4 were stopped at this point. These results indicated that separation was not restricted by our symmetry boundary conditions.

Figure 5 shows a comparison of the three steady-state numerical solutions in the wake region. Near the cylinder ($R/R_o < 3$) the two calculations using a finite outer boundary (cases 47-1 and 47-2) are in agreement. The calculations for case 47-3, using the coordinate mapping, predict higher densities near the cylinder than predicted by the first two cases. The calculations for cases 47-1 and 47-2 fail far downstream of the cylinder. These two cases predict large gradients of velocity, density and temperature far downstream. In the physical flow field large gradients would be present if there were a wake shock but would be opposite in sign to those predicted by these calculations. The large gradients predicted downstream in cases 47-1 and 47-2 are typical of those in rarefaction waves. These gradients result from the unnatural acceleration the flow experiences in the numerical solution by the specification of freestream boundary conditions downstream of the cylinder.

The numerical solution for case 47-3 predicts a more realistic qualitative behavior far downstream ($R/R_o > 10$). The large gradients are eliminated in this solution as a result of the asymptotic behavior of the coordinate mapping. None of the three steady-state solutions for $Re_d = 46.8$ predicted a wake shock downstream of the cylinder.

In cases 47-1 and 47-2 no density boundary condition was specified along the downstream portion of the outer boundary (refer to 4 in Figure 3). Both of these cases predict densities much lower than freestream at the outer boundary along $\theta = 180^\circ$. Case 47-3 predicts a density downstream which asymptotically approaches the freestream value. It thus appears that the mapping and boundary conditions used in case 47-3 produce better qualitative results downstream of the cylinder than the calculations prescribing freestream boundary conditions along the finite outer boundary.

Figure 6 shows the density distribution across the bow shock at its intersection with the stagnation streamline. The numerical solutions for $Re_d = 46.8$ predict shock thicknesses of two to three mean free paths. The analytical viscous normal shock solution of

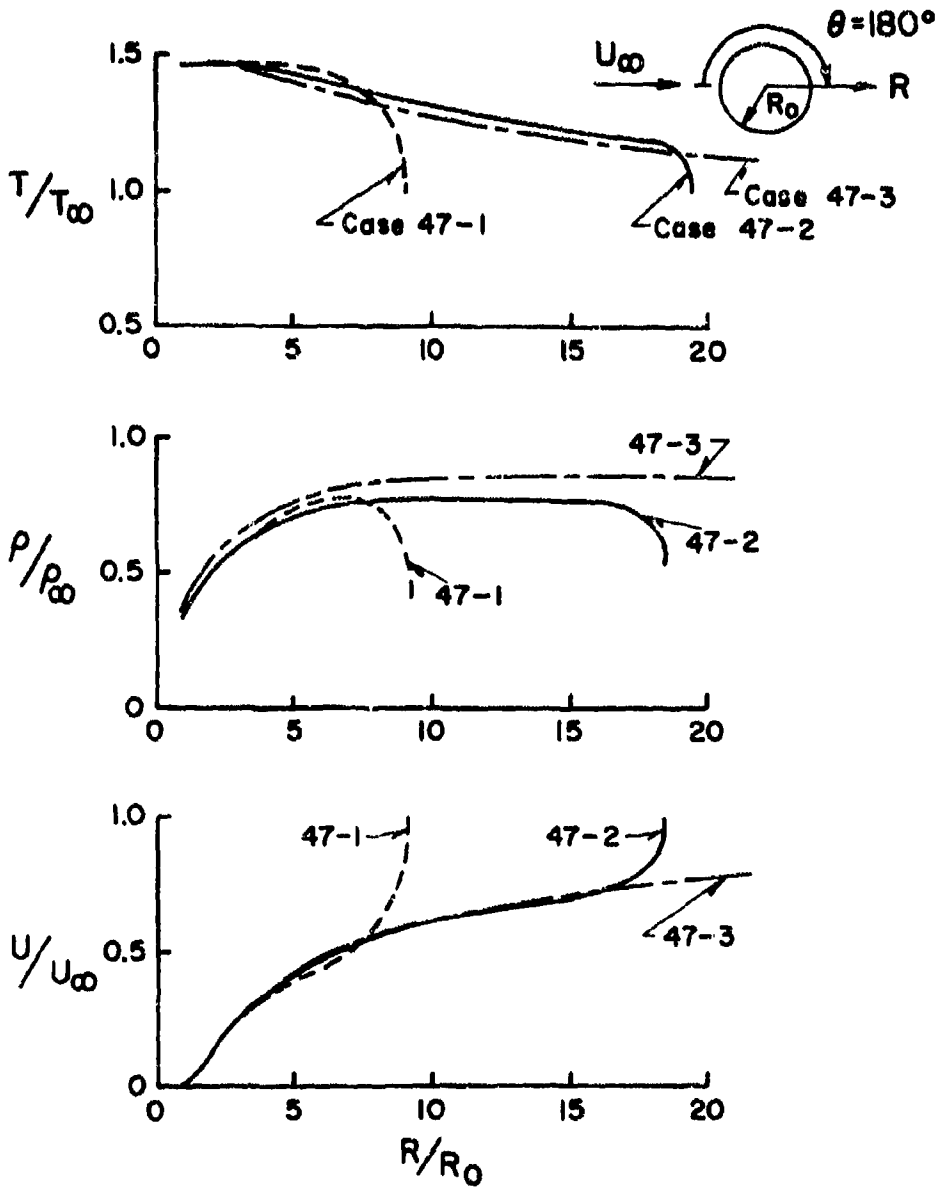

Figure 5. Flow Variables in Wake ($\theta = 180^{\circ}$) for $Re_d = 46.8$

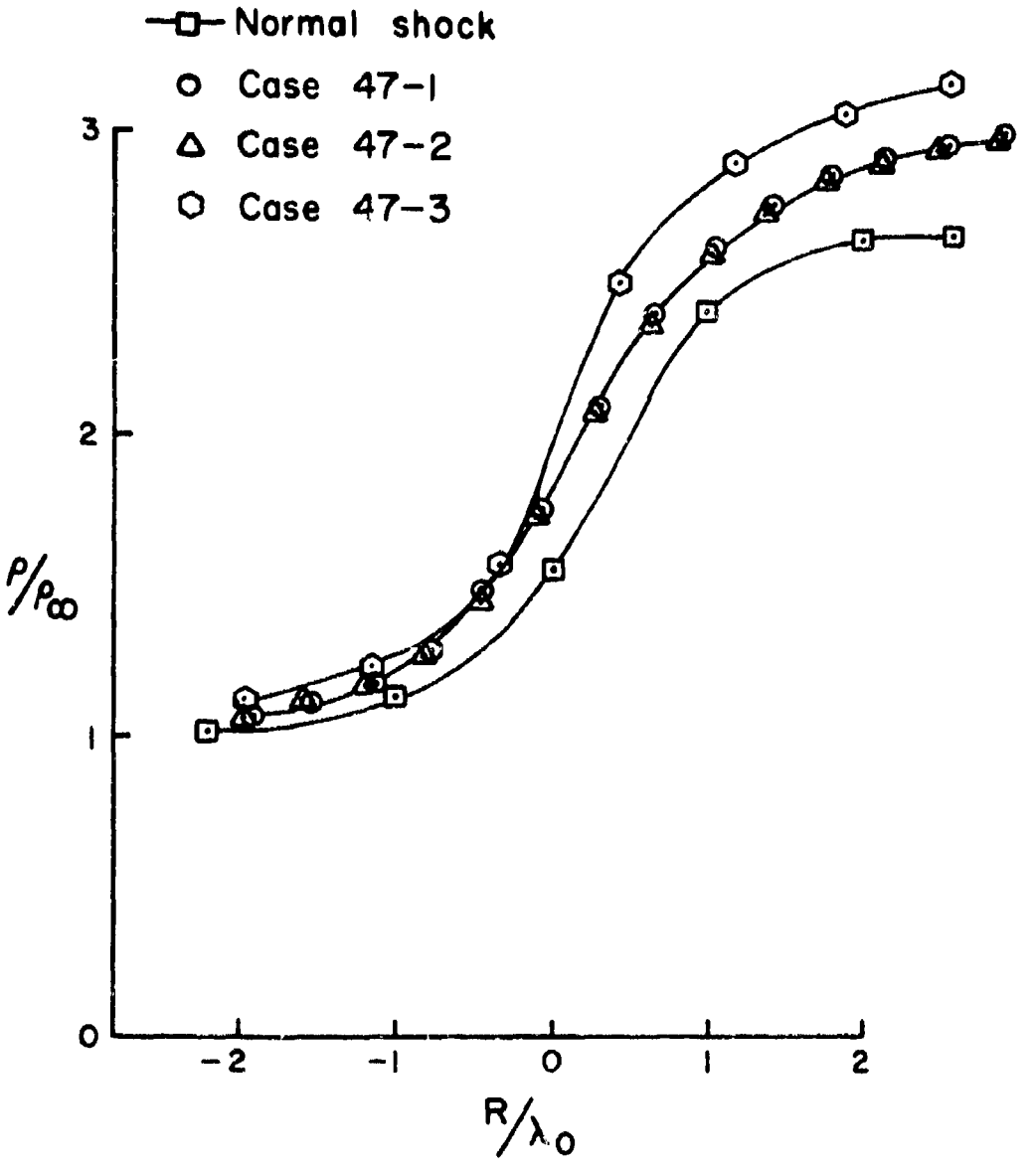

Figure 6. Shock Structure ($\theta = 0^{\circ}$) in Terms of Freestream Mean Free Paths for $Re_d = 46.8$

Morduchow and Libby[11] shown in this figure has a shock thickness of two mean free paths. The good resolution of the shock region in our numerical computations is due to the very fine difference mesh used in the bow shock region; less than one mean free path in the radial direction. Numerical solutions typically spread shocks over many mesh widths and thus predict innacurate shock thicknesses. Walitt[12] calculates shock thicknesses on the order of 90 mean free paths for Mach two flow at $Re_d = 1409$.

Figure 7 shows the time history of the density ratio across the bow shock at $\theta = 0^o$. The numerical calculations for case 47-1 predict a steady-state density ratio which is seven percent higher than that predicted analytically. The analytical solution used for comparison is the normal shock solution with first-order corrections for shock curvature due to Chow and Ting[13]. The numerical calculations for case 47-3 predict a steady-state density ratio which is 14 percent higher than this analytical solution. The Rankine-Hugoniot normal shock solution is also shown in Figure 7.

Figure 8 shows the density distribution along the stagnation streamline predicted by the three steady-state numerical solutions. Near the cylinder case 47-3 predicts much higher densities than either case 47-1 or 47-2. Case 47-2 is seen to predict a larger standoff distance than either of the other two cases. These results show that the manner in which the boundary conditions are specified for the numerical solutions has a very large influence on the density distribution predicted near the cylinder; both upstream and downstream.

None of the three steady-state calculations for $Re_d = 46.8$ showed any tendency toward separation as we would expect on the basis of the incompressible experimental results by Taneda[14]. His results show that for incompressible flow past cylinders a separation bubble forms downstream for Reynolds numbers above $Re_d \approx 5$. For Reynolds numbers above $Re_d \approx 45$ part of the separation bubble is shed alternately from each of the two recirculation regions. In the physical incompressible flow field symmetric separation is unstable for

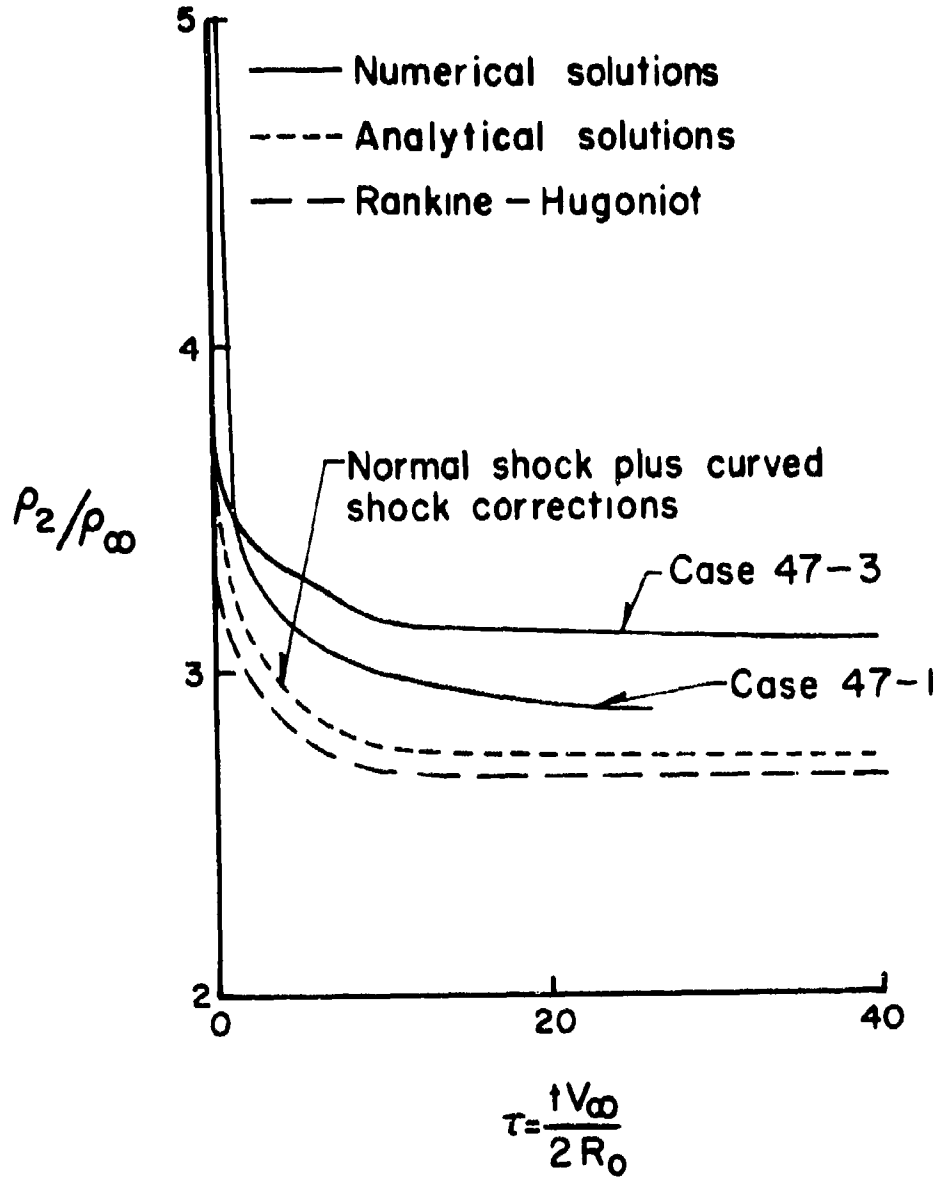

Figure 7. Time History of Density Ratio Across the Bow Shock ($\theta = 0^\circ$) for $Re_d = 46.8$

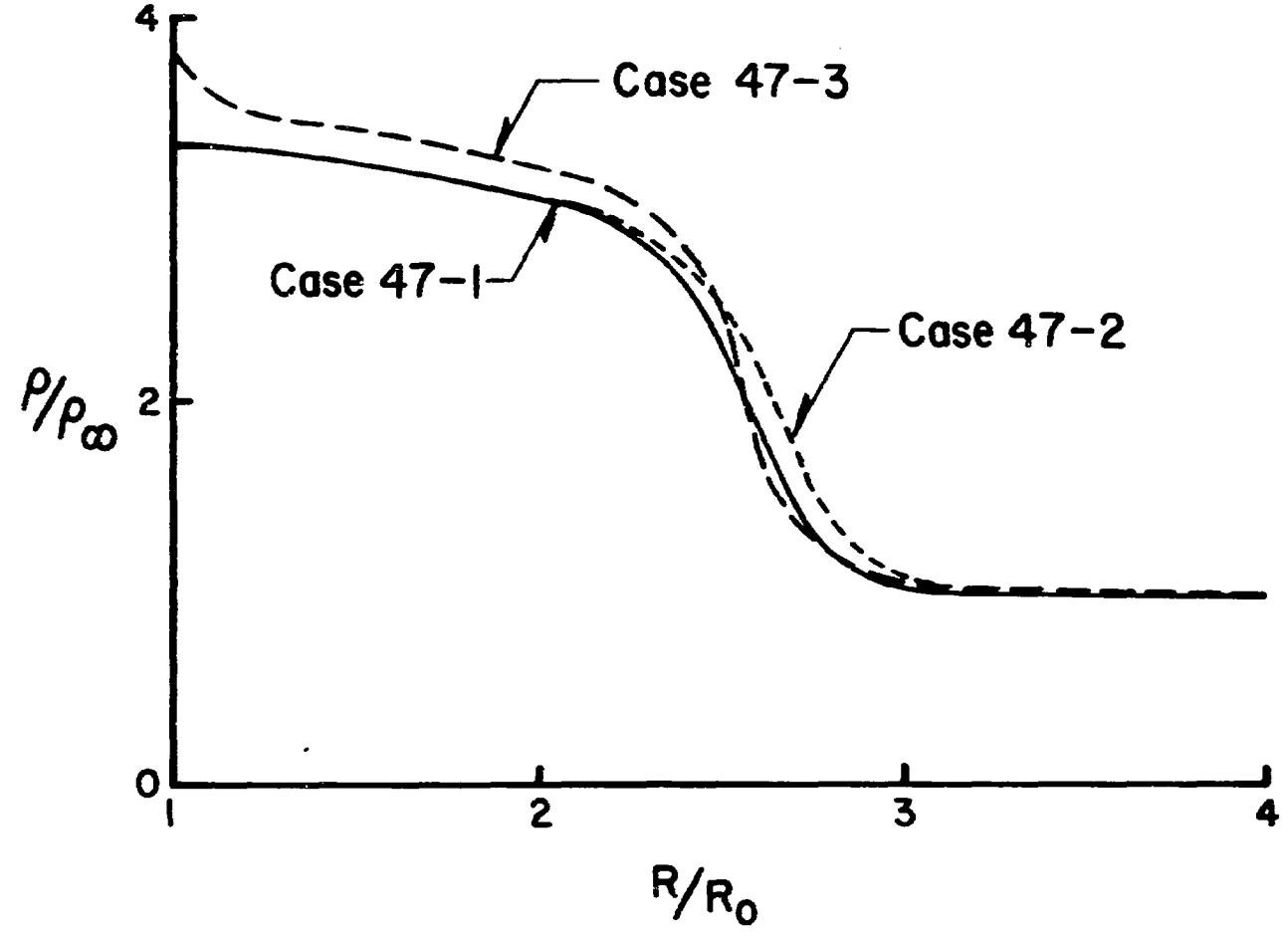

Figure 8. Steady-State Density Distribution Along Stagnation Streamline ($\theta = 0^\circ$) for $Re_d = 46.8$

Reynolds numbers above $Re_d \approx 45$. A calculation for $Re_d = 15.0$ was run to make certain that our symmetric downstream boundary conditions were compatible with the stability of the flow field.

C. $Re_d = 15.0$

The numerical calculations for $Re_d = 15.0$ employed the coordinate mapping (13) and the boundary conditions previously described for use with the mapping. The computations were started at time zero using the initial conditions for the impulsively accelerated cylinder. The steady-state solution was reached at $\tau = 47.7$ after 13 hours of computer time and approximately 3000 time steps.

The mesh size used in this computation was identical to that used for case 47-3. The density was the only freestream flow variable which differed from that used in case 47-3. Table.AI shows the values specified for the freestream flow quantities in this case.

The purpose of this low Reynolds number case was to determine if our specification of downstream symmetry boundary conditions restricted separation in the higher Reynolds number solutions described previously. The steady-state numerical solution for case 15 showed no tendency toward separation. It thus appears that our symmetry boundary condition is compatible with the numerical computation and does not prevent separation.

Figure 9 shows the steady-state density and temperature distributions along the stagnation streamline for $Re_d = 15.0$. The density ratio predicted by this numerical solution across the bow shock is 2.77. This is three percent higher than that predicted by the normal shock solution with first-order corrections for shock curvatuve[13]. The standoff distance predicted by this numerical solution is expectantly larger, approximately 45 percent larger than that predicted by the numerical calculations for $Re_d = 46.8$.

It is interesting to compare this solution for case 15 with the solution for case 47-3. Both of these cases employed the same mesh sizes with all freestream flow quantities identical except for the density. Cases 15 and 47-3 used identical initial conditions and

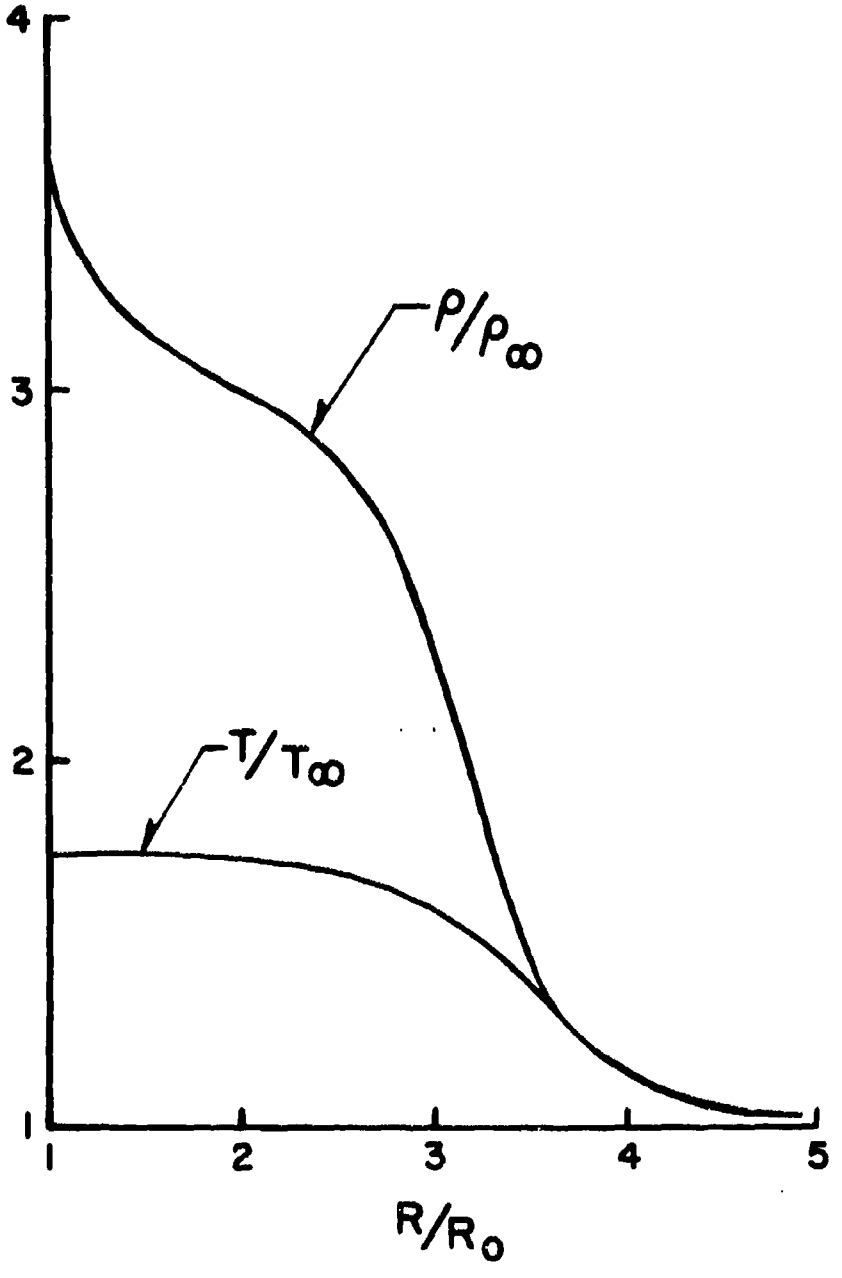

Figure 9. Steady-State Density and Temperature Distributions Along the Stagnation Streamline ($\theta = 0^{o}$) for Re_{d} = 15.0

boundary conditions and both used the coordinate mapping (13). The numerical solutions in the bow shock region are quite different. Case 47-3 predicts a density ratio across the bow shock which is much too high as described previously. Case 15 predicts a density ratio across the bow shock which is quite close to the analytical result.

Since both case 15 and case 47-3 use the same initial conditions, mapping, and boundary conditions it appears that the number of mesh points across the bow shock is the crucial difference between these two calculations. Case 15 has almost three times as many mesh points across the bow shock at $\theta = 0^{\circ}$ as case 47-3. This is because the gas mean free path is larger in case 15 and the shock is consequently thicker. Case 15 had 12 mesh points across the bow shock where it intersected the stagnation streamline (almost four mesh points per mean free path).

D. $Re_d = 157.2$

A numerical calculation was made for a Reynolds number of $Re_d = 157.2$. The purpose of this calculation was to obtain a numerical solution which could be compared with experimental wake measurements[8] taken for the same Mach number and Reynolds number. These hot-wire measurements taken downstream of a circular cylinder at $Re_d = 157.2$ in a Mach two freestream show that a wake shock is present in the flow field.

Several attempts were made to start the integration of case 157 at time zero using the "impulsive acceleration" initial conditions. These initial conditions produced excessive density ratios at the forward stagnation point on the cylinder. The density ratio reached values in excess of an order of magnitude larger than that for a flow undergoing an unsteady isentropic compression. Due to these inaccurate numerical results during the first few time steps this procedure was abandoned in favor of interpolation from another steady-state solution.

The numerical computation of case 157 was started at $\tau = 39.08$ by interpolating from the steady-state flow field of case 47-3. The free-stream density, velocity, and temperature used for case 157 were identical to that used in case 47-3. The viscosity relation used for case 157 was varied from that used in case 47-3 to produce a higher Reynolds number. Table AI shows the values used to prescribe the free-stream flow field.

The numerical solution reached the steady-state at $\tau = 58.14$ after nine hours of computer time and approximately 1500 time steps. Since the initial computations were performed by interpolating from a lower Reynolds number solution the time dependence for case 157 does not represent a cylinder accelerated from rest. The use of this interpolation technique for starting a solution offers a possible approach for obtaining an even higher Reynolds number solution in a reasonable amount of computer time.

The numerical computation for $Re_d = 157.2$ predicted a bow shock standoff distance of $\Delta/R_o = 1.282$. Figure 10 shows a comparison of the time history of the standoff distance for each calculation. The standoff distance calculated for $Re_d = 157.2$ is six percent larger than that predicted by inviscid calculations. Our numerical solutions predict that the standoff distance increases with decreasing Reynolds number. This variation of standoff distance is as we would expect.

The density ratio across the bow shock predicted by the numerical calculations for $Re_d = 157.2$ is much too large. At the point where the bow shock intersects the stagnation streamline a density ratio of $\rho_2/\rho_\infty = 3.5$ is predicted by the numerical computations. This is 29 percent larger than predicted analytically by viscous normal shock solutions corrected to account for shock curvature[13] The cause of this large discrepancy appears to be that more mesh points than we used are needed in the vicinity of the bow shock.

Figure 11 shows the density distribution through the bow shock along $\theta = 0^\circ$ in terms of the freestream mean free path. The numerical calculations for $Re_d = 157.2$ predict a shock thickness of approximately three mean free paths while the analytical viscous normal shock

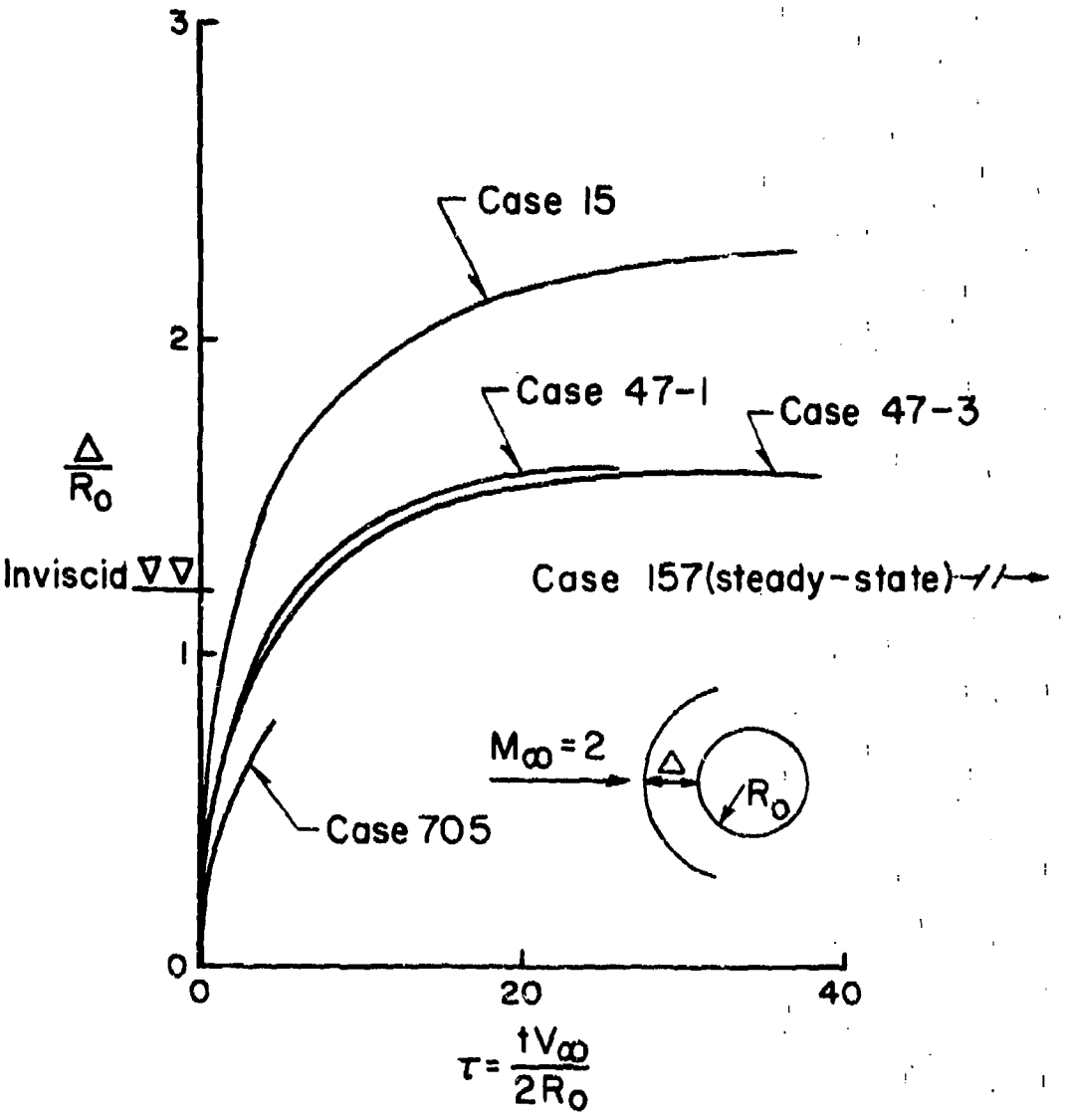

Figure 10. Time History of Bow Shock Standoff Distance

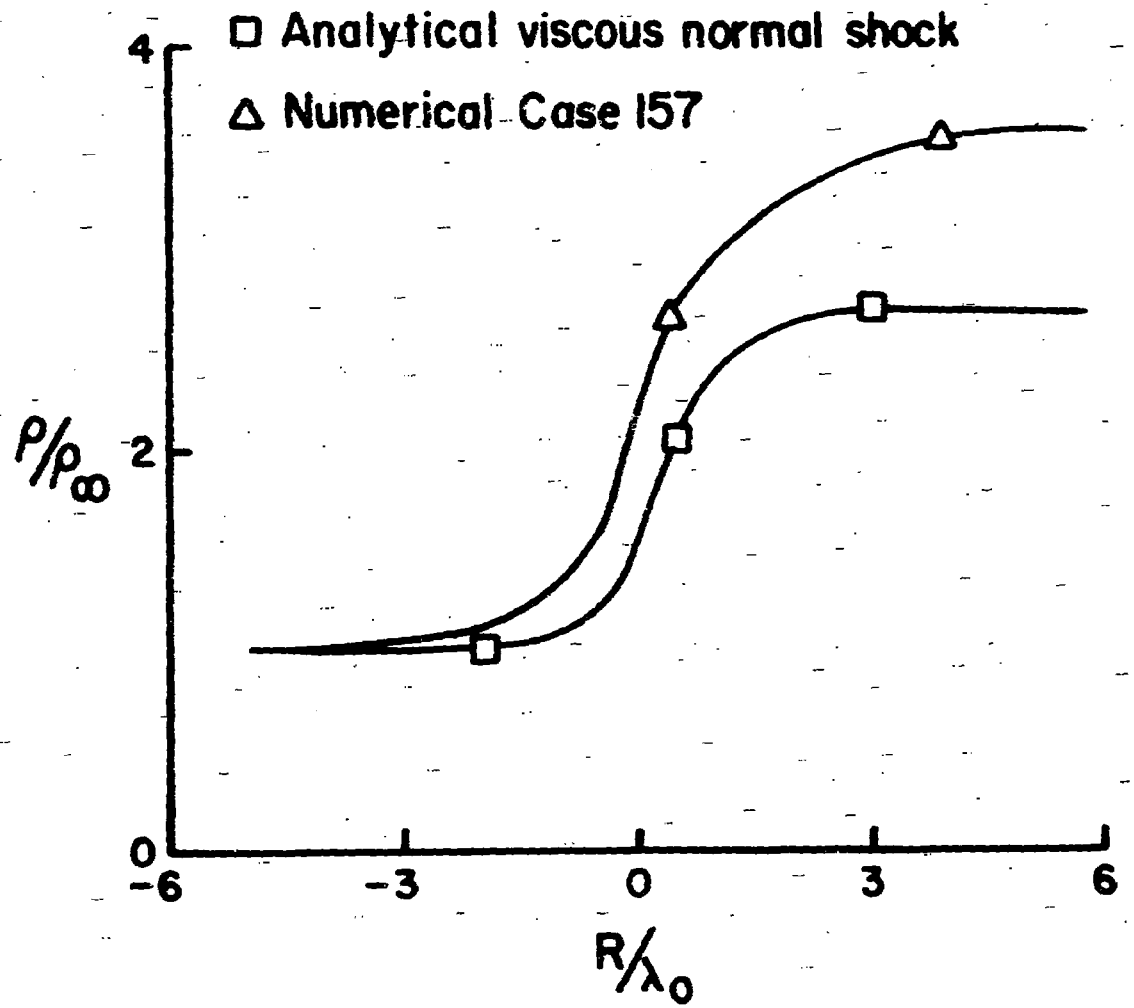

Figure 11. Shock Structure ($\theta = 0°$) in Terms of Freestream Mean Free Paths for $Re_d = 157.2$

solution[11] predicts a shock thickness of two mean free paths. Also apparent in Figure 11 is the large discrepancy between the Rankine-Hugoniot and numerical solution for the density ratio across the bow shock.

Figure 12 shows the pressure coefficient predicted throughout the flow field for case 157. Upstream of the cylinder ($X/R_o = -2$) the bow shock is quite pronounced By the time the flow reaches $X/R_o = 1$ the bow shock has been smeared over many mesh widths. This smearing or weakening of the bow shock is seen to continue as the flow moves downstream. The pressure coefficient at the forward stagnation point is $C_p = 2.29$. The bow shock is being smeared out by the asymptotic behavior of the coordinate mapping (13) used for the computations. This smearing or weakening of the bow shock is caused because free-stream conditions are specified at infinity and the condition

$$\partial/\partial R \to 0 \quad \text{as } R \to \infty \tag{19}$$

is inherent to the coordinate mapping (13). The approximate location of the wake shock is also shown in Figure 12 for reference.

Figure 13 shows the pressure coefficient in the wake region predicted by the numerical solution for case 157. Near the rear stagnation point ($\theta = 180^\circ$) the pressure is less than its freestream level. By the time the flow along the rear stagnation streamline reaches $X/R_o \sim 4$ its pressure level has exceeded that in the freestream. These profiles exhibit "shock-like" gradients in the wake region (i.e., $X/R_o = 3$, $Y/R_o \sim 1.5$). The dashed curve shown in Figure 13 represents the locus of points of maximum positive pressure gradient. Pressure increases as we cross this dashed line moving downstream. These gradients result from a compression of the flow and appear to represent the wake shock in the physical flow field. The numerical and experimental results[8] in the wake region cannot be compared directly since the experimental measurements were taken at $X/R_o \sim 70$ and the wake shock is smeared out in our numerical solution by $X/R_o \sim 13$ due to our placement of node points and the asymptotic

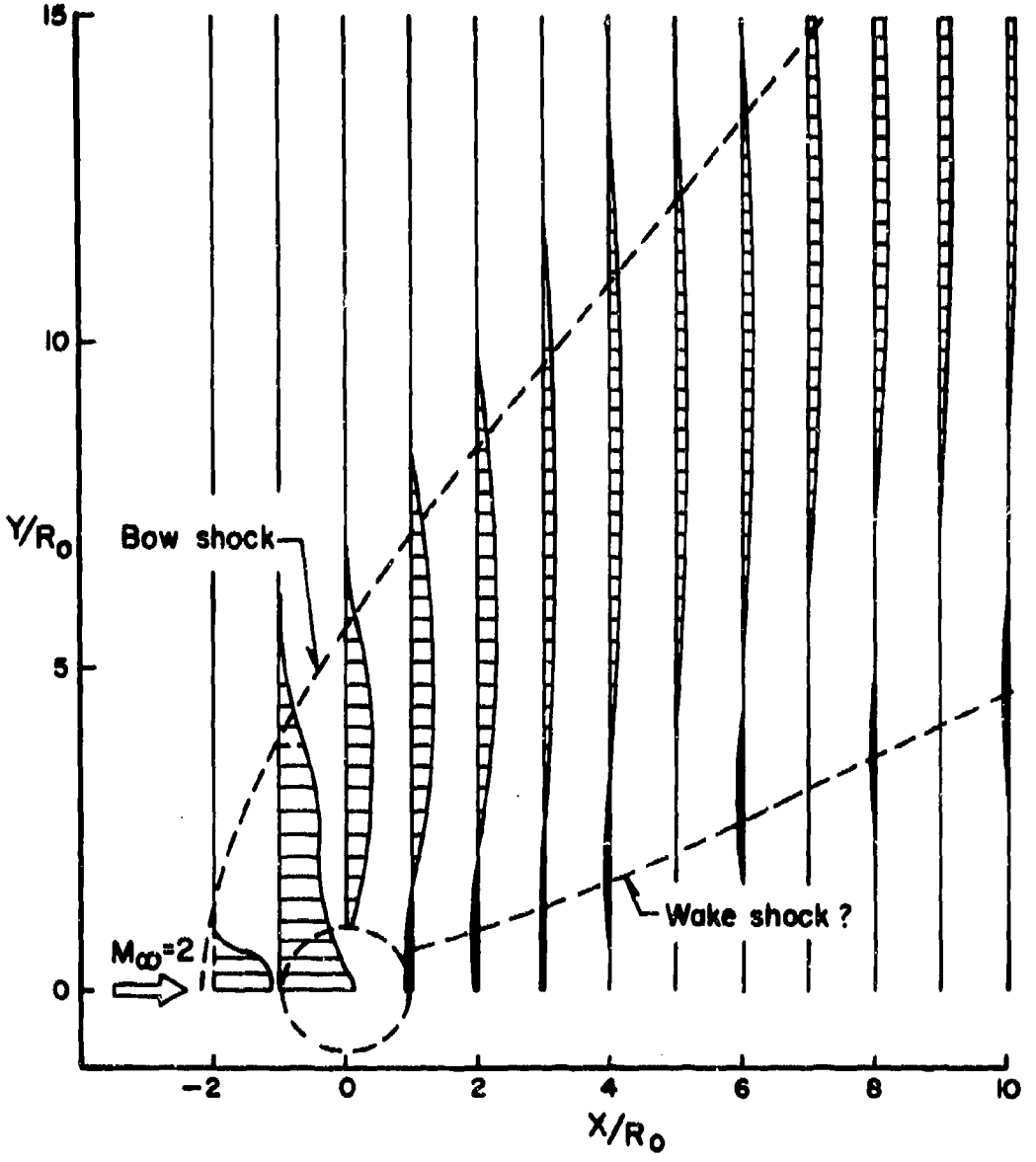

Figure 12. Numerical Solution for Pressure Coefficient for Re_d = 157.2

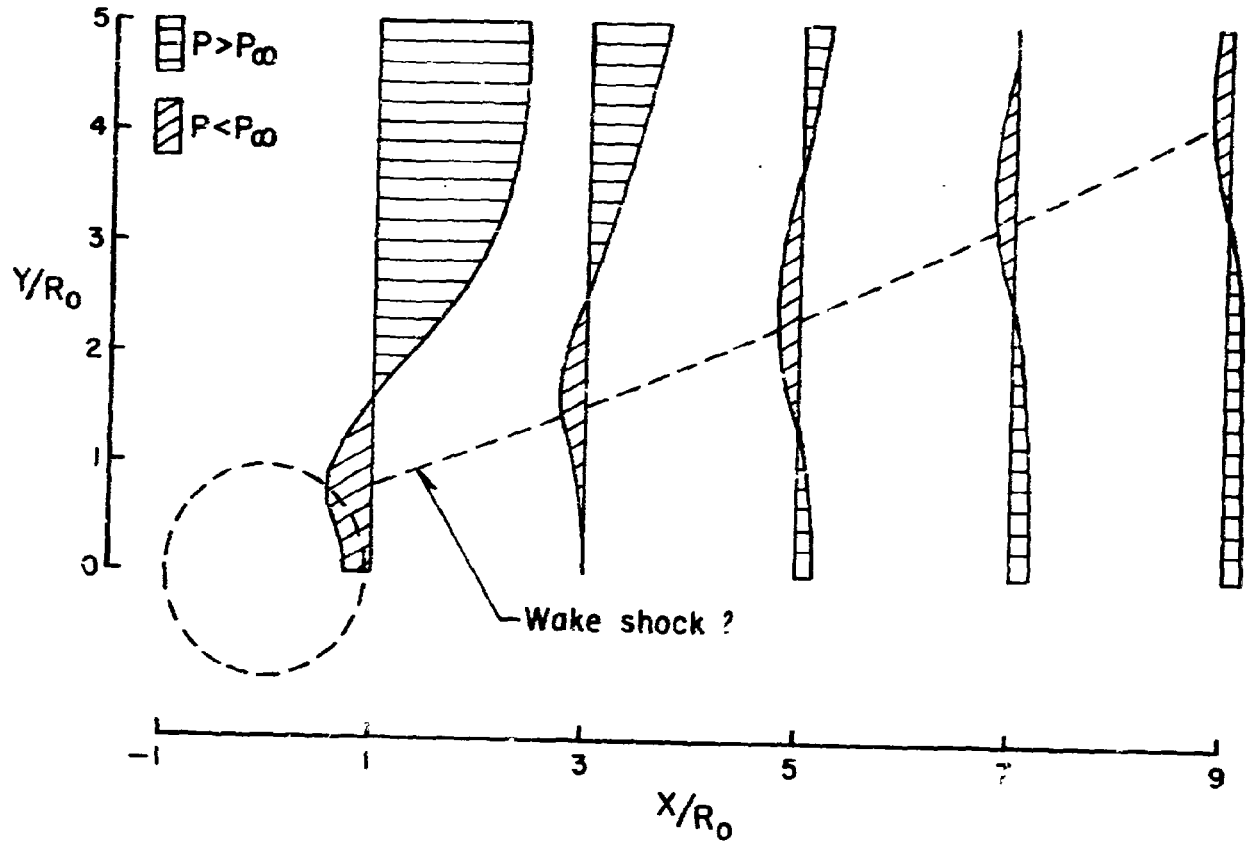

Figure 13. Numerical Solution for Pressure Coefficient in Wake for Re_d = 157.2

behavior of the coordinate mapping. We conclude that the numerical computations predict "shock-like" gradients in the wake at $Re_d = 157.2$ which may represent the wake shock present in the physical flow field at this same Reynolds number.

The numerical computations for $Re_d = 157.2$ predicted a small recirculation region downstream of the cylinder. The separation bubble predicted in these numerical calculations is shown in Figure 14. Separation is predicted to start at $\theta \sim 158^\circ$. On the basis of incompressible flow results this separation is very much delayed. For incompressible flow the separation point is located at $\theta \sim 109^\circ$. At the present time it is not known whether this delayed separation is a result of compressibility effects or errors in the numerical computations. It should be noted that the numerical computations for $Re_d = 15.0$ and 46.8 predicted no separation bubble downstream of the cylinder.

VI. CONCLUSIONS

This report has described a series of numerical experiments for the purpose of evaluating the accuracy of typical numerical solutions of the full Navier-Stokes equations. A computer program developed by Scala and Gordon[1] was used in this study to solve for the steady-state flow field around cylinders accelerated to supersonic velocities. Steady-state solutions were obtained for Mach two flow past cylinders at Reynolds numbers of 15.0, 46.8, and 157.2.

Our computations have shown that the density levels predicted downstream of the bow shock are higher than we would expect on the basis of analytical normal shock solutions corrected to account for shock curvature[15]. The degree of error present in our numerical solutions is closely linked to the spacing of mesh points in regions where large gradients are present. The steady-state calculations for $Re_d = 15.0$ had 12 mesh points across the bow shock and had three percent too high a density ratio; the calculation for $Re_d = 157.2$ had 29 percent too high a density ratio but only 5 mesh points across

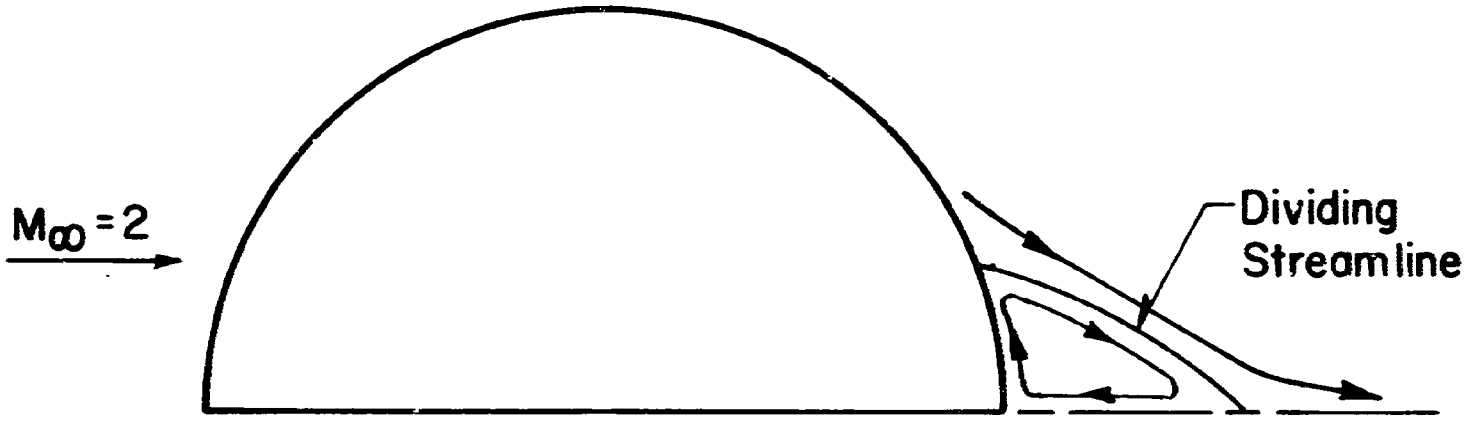

Figure 14. Separation Bubble in Numerical Calculations for Re_d = 157.2

the bow shock. It thus appears necessary to use very fine mesh spacings in flow regions having large gradients for accurate numerical calculations. Three or four mesh points per mean free path appear to be necessary in the region of the bow shock.

The numerical solutions for $Re_d = 15.0$ and 46.8 did not predict separation. The computation for $Re_d = 157.2$ predicted a small separation bubble on the downstream side of the cylinder. For this case separation began at $\theta = 180^\circ$ then the separation point shifted with time reaching a steady-state position at $\theta \sim 158^\circ$ Our numerical results thus predict very late separation compared to incompressible flow past a cylinder. Walitt[12] predicts separation at $\theta \sim 141^\circ$ in a numerical calculation for Mach two flow past a cylinder at $Re_d = 1409$. The accuracy of our numerically predicted separation point is unknown.

Steady-state numerical solutions were obtained for $Re_d = 15.0$, 46.8 and 157.2 by employing the coordinate mapping suggested by Sills[10]. Our calculations have shown that this coordinate mapping is compatible with initial-boundary-value problems of the present type. This mapping smooths out gradients far from the body. This smoothing process is beneficial in the wake region. The mapping eliminated the large unnatural gradients which resulted from specifying "artificial" freestream conditions downstream of the cylinder. The two methods of specifying boundary conditions downstream are discussed and compared in the calculations for $Re_d = 46.8$.

Experimental wake measurements[8] at $Re_d = 157.2$ have shown that a wake shock is present in Mach two flow at this Reynolds number. Our numerical computations for $Re_d = 157.2$ predict large pressure and temperature gradients at the edge of the inner wake which appear to be the numerical equivalent of the wake shock in the physical flow field. It is not clear, however, that the details of the wake region are accurately predicted by these calculations. The numerical calculations for $Re_d = 15.0$ and 46.8 predicted no wake shock. There is no experimental data for Reynolds numbers as low as 46.8.

The present numerical experiments have been for cylinders of approximately 1/32 inch and 1/2 inch diameter. To maintain a desired level of accuracy the number of mesh points used in a computation must increase if larger cylinders are considered. In view of the large computer times required for our calculations these small cylinder sizes represent an upper limit of our present capability. The calculation of a typical steady-state solution required from nine to eighteen hours on the BRLESC II computer. For a given problem it is impossible to predict in advance the degree of error which will be present in the steady-state numerical solution. Our computations have shown that errors of ten to twenty percent may result in numerical solutions of the Navier-Stokes equations even under carefully controlled conditions.

REFERENCES

1. S. M. Scala and P. Gordon, "Solutions of the Navier-Stokes Equations for Viscous Supersonic Flows Adjacent to Isothermal and Adiabatic Surfaces," General Electric Report 69SD1001, Philadelphia, Pennsylvania, April 1969.

2. L. Crocco, "Solving Numerically the Navier Stokes Equations," General Electric Report 63SD891, Philadelphia, Pennsylvania, March 1964.

3. H. U. Thommen, "A Method for the Numerical Solution of the Complete Navier-Stokes Equations for Steady Flows," General Dynamics Report GDC-ERR-AN733, San Diego California, April 1965.

4. S. M. Scala and P. Gordon, "Solution of the Time-Dependent Navier-Stokes Equations for the Flow Around a Circular Cylinder," AIAA J., Vol 6, No 5, May 1968, pp 815-822.

5. J. S. Allen and S. I. Cheng, "Numerical Solutions of the Compressible Navier-Stokes Equations for the Laminar Near Wake," The Physics of Fluids, Vol 13, No 1, January 1970, pp 37-51.

6. J. G. Trulio and L. Walitt, "Numerical Calculations of Viscous Compressible Fluid Flow Around A Stationary Cylinder, NASA CR-1465, January 1970.

7. J. G. Trulio and L. Walitt, "Numerical Calculation of Viscous Compressible Fluid Flow Around An Oscillating Rigid Cylinder," NASA CR-1467, October 1969.

8. C. W. Kitchens and C. C. Bush, "Hot-Wire Measurements in a Cylinder Wake for Low Reynolds Number Flow at Mach Two" Ballistic Research Laboratories Memorandum Report No. 2116, July 1971.

9. P. Gordon, "Nonsymmetric Difference Equations", SIAM J., Vol 13, No 3, September 1965, pp 667-673.

10. J. A. Sills, "Transformations for Infinite Regions and Their Applications to Flow Problems," AIAA J., Vol 7, No 1, January 1969, pp 117-123.

11. M. Morduchow and P. Libby, "On A Complete Solution of the One-Dimensional Flow Equations of a Viscous, Heat Conducting, Compressible Gas", J. Aero. Sci., Vol 16, No 11, November 1949, pp 674-684.

12. L. Walitt, "Numerical Studies of Supersonic Near-Wakes," Ph.D. Thesis, University of California, Los Angeles, California, 1969.

13. R. Chow and L. Ting, "Higher-Order Theory of Curved Shock," Aeronautical Research Laboratory TN 60-142, August 1960.

14. S. Taneda, "Experimental Investigation of the Wakes Behind Cylinders and Plates at Low Reynolds Numbers," J. Phys. Soc. Japan, Vol 11, No 3, March 1956, pp 302-307.

APPENDIX A

The following gas properties were held fixed for all the numerical cases considered

$$R = 5.52 \times 10^{1} \text{ ft-lb}_f/\text{lb}_m - {}^{\circ}\text{R} , \tag{A1}$$

$$c_v = 1.38 \times 10^{2} \text{ ft-lb}_f/\text{lb}_m - {}^{\circ}\text{R} , \tag{A2}$$

$$\gamma = 1.40 . \tag{A3}$$

The freestream Reynolds number was varied by changing the cylinder size or freestream conditions of the flow. The specific values used for each case are shown in Table A-I. These dimensional variables are input quantities for the computer program developed by Scala and Gordon[1]. Each case is specified by its approximate Reynolds number. The four cases for $Re_d = 46.8$ are differentiated by a numerical suffix (i.e. 47-1). Table A-I also shows which calculations were performed using the coordinate mapping and the number of mesh points used for each calculation.

TABLE A-I Dimensional Values of Freestream Variables and Size of Computation

Case	705	47-1	47-2	47-3	47-4	15	157
U_∞, ft/sec	290.45	290.45	290.45	2904.50	2904.50	2904.50	2904.50
T_∞, ^oR	8.468	8.468	8.468	8.46.8	846.8	846.8	846.8
ρ_∞ lb_m/ft^3	$1.964x10^{-4}$	$1.964x10^{-4}$	$1.964x10^{-4}$	$1.964x10^{-4}$	$1.964x10^{-4}$	$6.295x10^{-5}$	$1.964x10^{-4}$
R_o ft	$2.30x10^{-2}$	$1.528x10^{-3}$	$1.528x10^{-3}$	$1.528x10^{-3}$	$1.528x10^{-3}$	$1.528x10^{-3}$	$1.528x10^{-3}$
$\mu T^{-1/2}$, $lb_m/ft\text{-}sec$	$1.28x10^{-6}$	$1.28x10^{-6}$	$1.28x10^{-6}$	$1.28x10^{-6}$	$1.28x10^{-6}$	$1.28x10^{-6}$	$3.81x10^{-7}$
$kT^{-1/2}$ $lb_f/^oR\text{-}sec$,	$3.49x10^{-4}$	$3.49x10^{-4}$	$3.49x10^{-4}$	$3.49x10^{-4}$	$3.49x10^{-4}$	$3.49x10^{-4}$	$1.039x10^{-4}$
Number of Mesh Points	3007	1209	2945	1209	2379	1209	1581
Coordinate Mapping to ∞	No	No	No	Yes	Yes	Yes	Yes